Rare Metal Materials and Engineering
Volume 51, Issue 5, May 2022
Available online at www.rmme.ac.cn

Science Press

Cite this article as: Shao Minghao, Zhang Jian, Wang Weiping, et al. Corrosion Behavior of Self-Reacting Friction Stir Welded AA2219-T87 Aluminum Alloy[J]. Rare Metal Materials and Engineering, 2022, 51(05): 1620-1626.

ARTICLE

Corrosion Behavior of Self-Reacting Friction Stir Welded AA2219-T87 Aluminum Alloy

Shao Minghao[1], Zhang Jian[2], Wang Weiping[3], Liu Debo[2], Guo Qilong[1], Zhang Hua[1]

[1] School of Mechanical Engineering, Beijing Institute of Petrochemical Technology, Beijing 102617, China; [2] Beijing Institute of Aerospace Systems Engineering, Beijing 100076, China; [3] Regional Representative Office in Chengdu, Chengdu 610100, China

Abstract: The corrosion behavior of different regions of AA2219-T87 aluminum alloys after self-reacting friction stir welding was investigated through the electrochemical corrosion and immersion corrosion tests. The results show that the weld nugget zone (WNZ) has the optimal corrosion resistance, while the base material shows the worst corrosion resistance. In the base material, the volume fraction of precipitated phase is the largest. The closer the area to the nugget center, the more the dissolving precipitated phase. WNZ is composed of fine equiaxed grains with a small amount of θ phase.

Key words: self-reacting friction stir welding; aluminum alloy; corrosion behavior; corrosion resistance

The AA2219 aluminum alloys are widely used in the aerospace industry as fuel tanks of large carrier rocket[1,2]. The friction stir welding (FSW) is a common method to weld aluminum alloys, which results in relatively small welding deformation and few cracks, air holes, and inclusions in the welded zone[3,4]. Maintaining the required pressure during FSW is difficult to weld large and complex components. Besides, the backing plate is required in the welding process, the keyhole needs to repair after FSW, and the root flaws may occur, which all restrict the application of FSW. Thus, the self-reacting friction stir welding (SR-FSW), i. e., bobbin-tool friction stir welding (BT-FSW), is proposed. Fig. 1 illustrates the welding method of SR-FSW process[5]. The side of the weld joint is advancing side (AS), and the other side is retreating side (RS). SR-FSW does not require the rigid support, which is appropriate for the girth seam welding of rocket storage tanks. No keyhole after SR-FSW indicates no further repairment. Moreover, SR-FSW has lower rotation speed and higher travel speed, compared with FSW, thereby increasing the welding efficiency[6,7].

The welded products with minimal defects, improvement in welding processes[8,9], uniform temperature or stress distribution during welding, proper microstructure, and high corrosion resistance[10,11] have been widely studied. However, the corrosion behavior of joint after SR-FSW is rarely researched, which needs further investigation[12,13]. Ref.[14-16] reported the corrosion and protection of welded joints. In this research, the corrosion behavior of AA2219-T87 aluminum alloys after SR-FSW was studied through the electrochemical corrosion and immersion corrosion tests. The corrosion resistance and microhardness of base material (BM), heat-affected zone (HAZ)/thermal-mechanically affected zone (TMAZ), and welding nugget zone (WNZ) in welded joints were also discussed.

1 Experiment

The AA2219-T87 aluminum alloy with 6 mm in thickness was used in this study, and Table 1 shows its chemical composition. SR-FSW with a rotation speed of 300 r/min and the linear speed of 400 mm/min was used to prepare the welded joints. The pin tool has the upper and lower shoulders with 20 mm in diameter and a cylindrical pin with 8 mm in diameter.

The welded plates were cut into the specimens of 10 mm× 100 mm×6 mm. After grinding and polishing, the specimens were etched by Keller reagent (95 mL water+2.5 mL HNO_3+ 1.5 mL HCl+1.0 mL HF) at room temperature for 90~180 s. The optical microscope (OM) of Nikon ECLIPSE MA200

Received date: May 25, 2021
Foundation item: National Natural Science Foundation of China (51774047)
Corresponding author: Zhang Hua, Ph. D., Professor, School of Mechanical Engineering, Beijing Institute of Petrochemical Technology, Beijing 102617, P. R. China, Tel: 0086-10-81292220, E-mail: huazhang@bipt.edu.cn

was used to observe the metallographic morphology. In addition, the transmission electron microscope (TEM) was used to study the metallurgical changes associated with welding. Vickers hardness of the welded cross-sections was measured from the top to the bottom at different points, as shown in Fig.2.

The electrochemical measurement tests were performed in 3.5wt% NaCl solution with a typical three-electrode system using the electrochemical corrosion workstation OGF500. Pt was used as the auxiliary electrode, the saturated calomel electrode (SCE) was regarded as the reference electrode, while the working electrode was BM, HAZ/TMAZ, or WNZ. In addition, the area of the specimen exposed in the solution was processed according to ASTM G69-12.

The immersion corrosion tests were also conducted in 3.5wt% NaCl solution. The specimen with different zones is shown in Fig. 3. The zone F is BM, zone A and zone E are HAZ, zone B is the shoulder edge of AS, and zone D is the shoulder edge of RS. During the practical application, the top surface is exposed to the environment, so it is chosen as the investigated object. To study the electrochemical behavior of each area, five regions were selected on the top surface, and the rest was coated by strippable paint based on GB10124-88. Each test was conducted at the ambient temperature for 3 weeks, 1 month, 2 months, 4 months, and 6 months.

To remove the corrosion products on the tested specimens, the solution of 50 mL H_3PO_4 (ρ=1.69 g/mL), 20 g CrO_3, and 1000 mL deionized water was used, according to ASTM G1-03. Then the specimens were rinsed with running water and ethanol. Scanning electron microscope (SEM) was used to study the corrosion morphology in different zones of the welded joints.

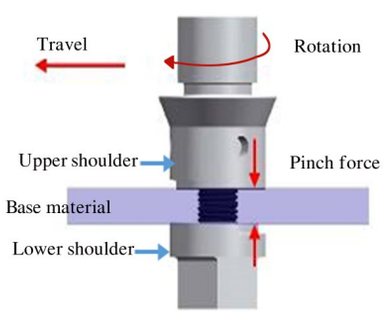

Fig.1 Schematic diagram of SR-FSW process[5]

Table 1 Chemical composition of AA2219-T87 aluminum alloys (wt%)

Cu	Si	Fe	Mn	Mg	Zr	Zn	Ti	V	Al
6.40	0.20	0.30	0.30	0.02	0.15	0.10	0.07	0.11	Bal.

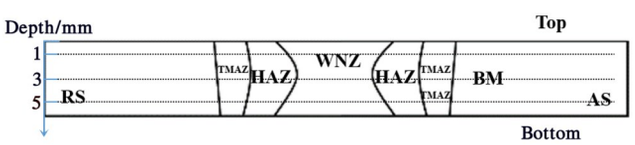

Fig.2 Schematic diagram of cross-section of welded joint

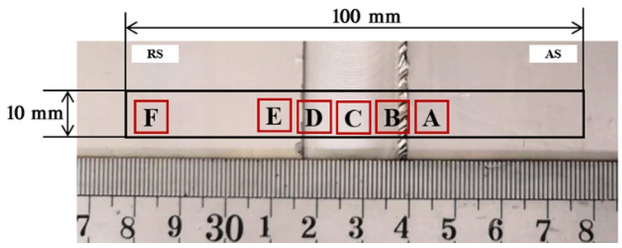

Fig.3 Immersion corrosion specimen with different zones

2 Results

2.1 Microstructure and microhardness

Fig.4 shows the cross-section microstructures of BM, HAZ, and WNZ. It can be seen that WNZ consists of fine grains: the original grains are broken, the dynamic recrystallization occurs, and thus the grains are greatly refined. BM zone consists of large elongated grains. The microstructure changes of HAZ-AS and HAZ-RS along the rotation direction indicate that the grains are coarsened and their shape is changed during SR-FSW process due to the thermal and mechanical effects. These results are in good agreement with those in Ref. [17,18].

Fig. 5a shows the microhardness variation of upper and lower surfaces of welded specimens. The typical W-shaped curve of microhardness can be observed. Because the top and bottom surfaces were heated at the same temperature, there is little difference in their microhardness. Fig. 5b shows the microhardness of specimens along the depth direction, which also suggests no significant difference in microhardness of different layers because of the similar thermal processes.

2.2 Electrochemical corrosion

Fig.6 shows the open-circuit potential (OCP) curves of BM, HAZ/TMAZ, and WNZ. The potential difference of BM is the lowest of −0.71 V. The measured potential difference of HAZ/TMAZ is −0.68 V, which is close to that of BM because of their similarities in grain size and phase distributions. The potential difference of WNZ is stable at −0.62 V, which is noticeably different from that of BM and HAZ/TMAZ. Therefore, WNZ has the optimal corrosion resistance, followed by HAZ/TMAZ, and BM has the worst corrosion resistance.

Fig. 7 shows the potentiodynamic polarization curves of BM, HAZ/TMAZ, and WNZ. The curves were derived using Tafel method. The corrosion potential E_{corr} presents a variation trend which is similar to that of OCP curves: E_{corr} of WNZ, HAZ/TMAZ, and BM is −0.622, −0.682, and −0.719 V, respectively. WNZ has the most positive corrosion potential, indicating the most stable zone of the welded joints, followed by HAZ/TMAZ and BM. In general, BM shows the more inferior corrosion resistance, which is in agreement with Ref. [19,20].

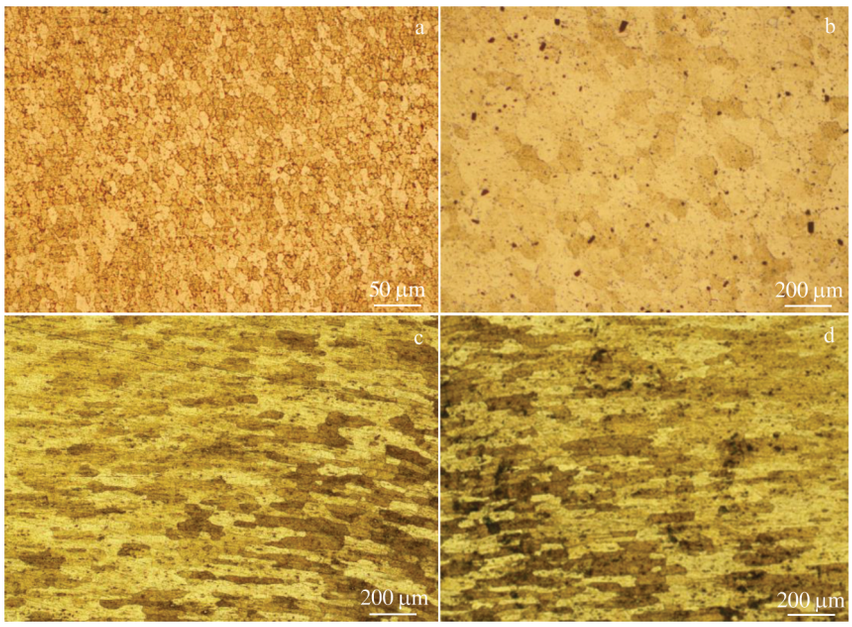

Fig.4 Cross-section microstructures of different zones in welded joints of AA2219-T87 Al alloys after SR-FSW: (a) WNZ, (b) BM, (c) HAZ-AS, and (d) HAZ-RS

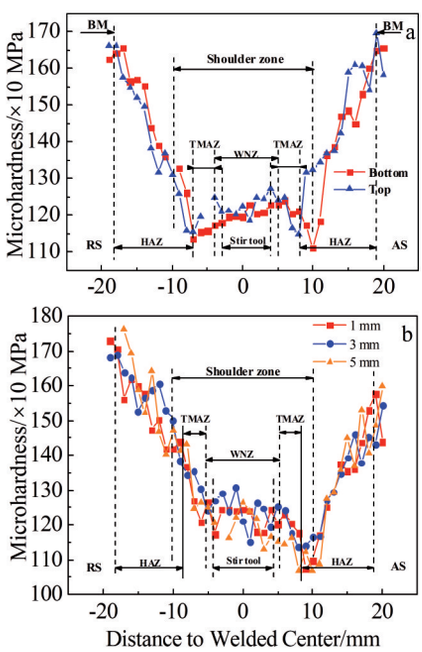

Fig.5 Microhardness of shoulder surfaces (a) and cross-section along depth direction (b) of welded joints

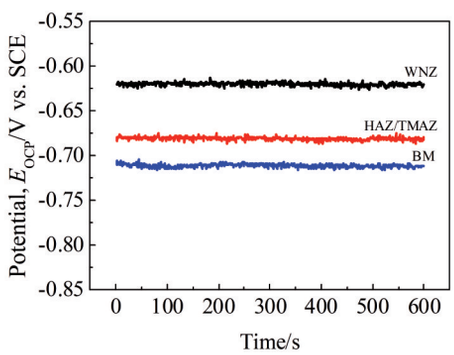

Fig.6 Open circuit potential of WNZ, HAZ/TMAZ, and BM of welded joints

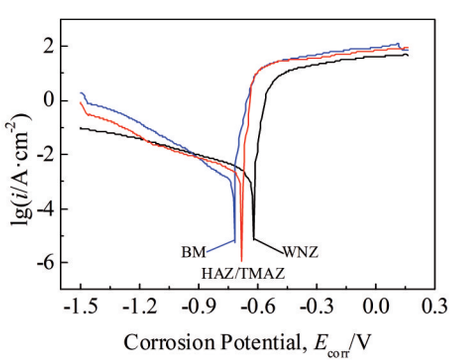

Fig.7 Potentiodynamic polarization curves of WNZ, HAZ/TMAZ, and BM of welded joints

2.3 Immersion corrosion

To further compare the corrosion resistance, the immersion corrosion tests were conducted on BM, HAZ-AS, HAZ-RS, and WNZ regions. Fig.8 shows the corrosion morphologies of BM. After immersion corrosion for 3 weeks, a large number of small and shallow etch pits appear on the surface, which account for 11.45% of surface area. The depth and width of etch pits are expanded with the corrosion proceeding. After 6 months, many deep etch pits can be observed, which account for 95.17% of the surface area. The etch pits are connected to each other, and serious corrosion occurs on BM surface.

Fig. 9 shows the etching morphologies of HAZ-AS and HAZ-RS. The etching behavior of HAZ-AS or HAZ-RS is not

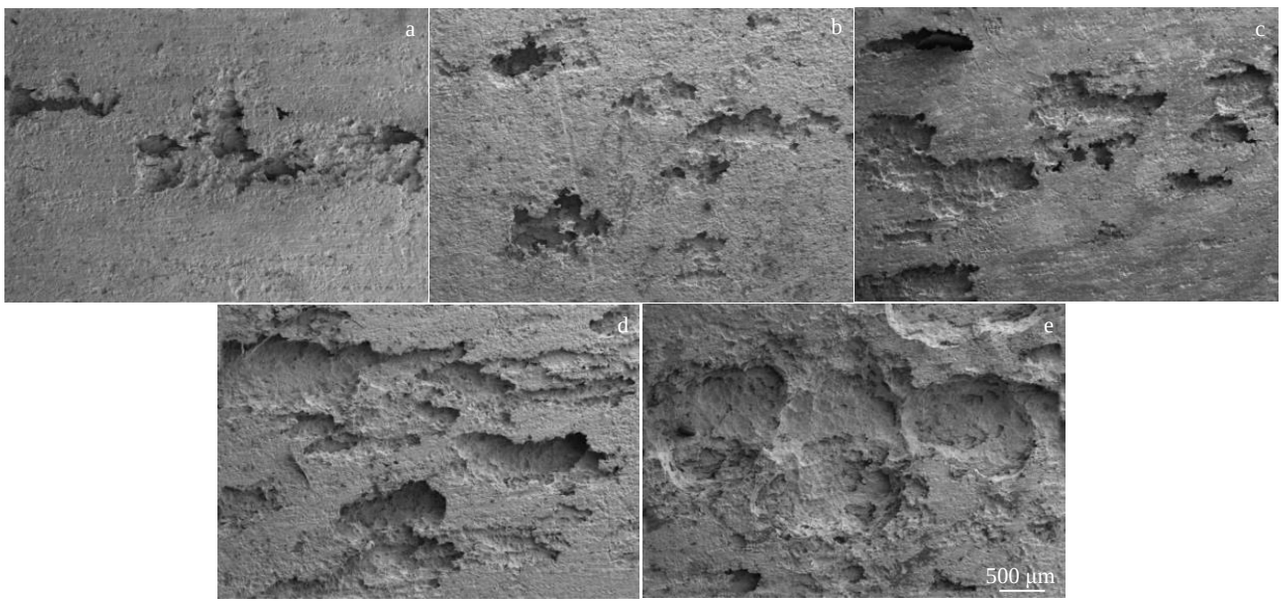

Fig.8 Etching morphologies of BM after immersion corrosion for 3 weeks (a), 1 month (b), 2 months (c), 4 months (d), and 6 months (e)

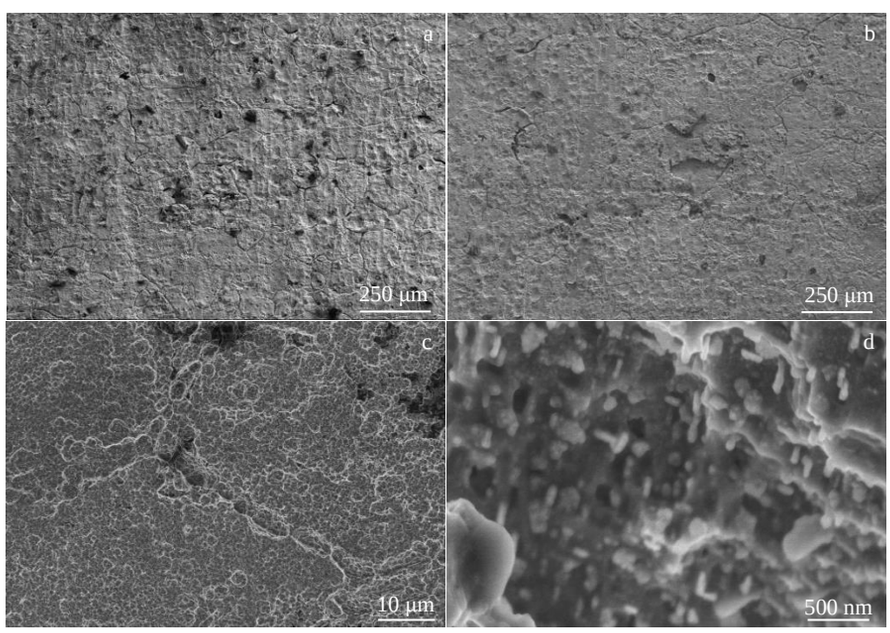

Fig.9 Morphologies of HAZ-AS (a) and HAZ-RS (b) and magnified corrosion morphologies (c, d) of welded joints after immersion corrosion for 6 months

significantly different. Neither of them shows more visible pits after immersion corrosion for 6 months, and only some small shallow holes appear on the surface. The etch pits on HAZ-RS are slightly more obvious than those on HAZ-AS. The small sub-circular pits are 23~40 μm in diameter on both sides. Fig. 9c reveals that the surface also has some connected sub-circular and superimposed shapes, but the corrosion state is not as severe as that of BM. As shown in Fig. 9d, there are many rods and white particles attached to the etch pit surface.

Fig. 10 presents the corrosion morphologies of WNZ without obvious surface pits, indicating the better corrosion resistance than that of HAZ. After immersion corrosion for 2~6 months, some small pits on WNZ surface (Fig. 10b) are gradually converted into irregularly shaped joints (Fig. 10c), thereby leading to the corrosion shedding on the central section (Fig. 10d). The corrosion behavior is also not clearly distinguished between HAZ-AS and HAZ-RS regions.

Due to the axial force of the shoulder during SR-FSW, many equally spaced arcs appear on the welded surface, as indicated by the arrows in Fig. 10a. Since the arc density extruded by the shoulder is less than that of the flat area, it can be seen from Fig. 10e that the arc top has a worse corrosion

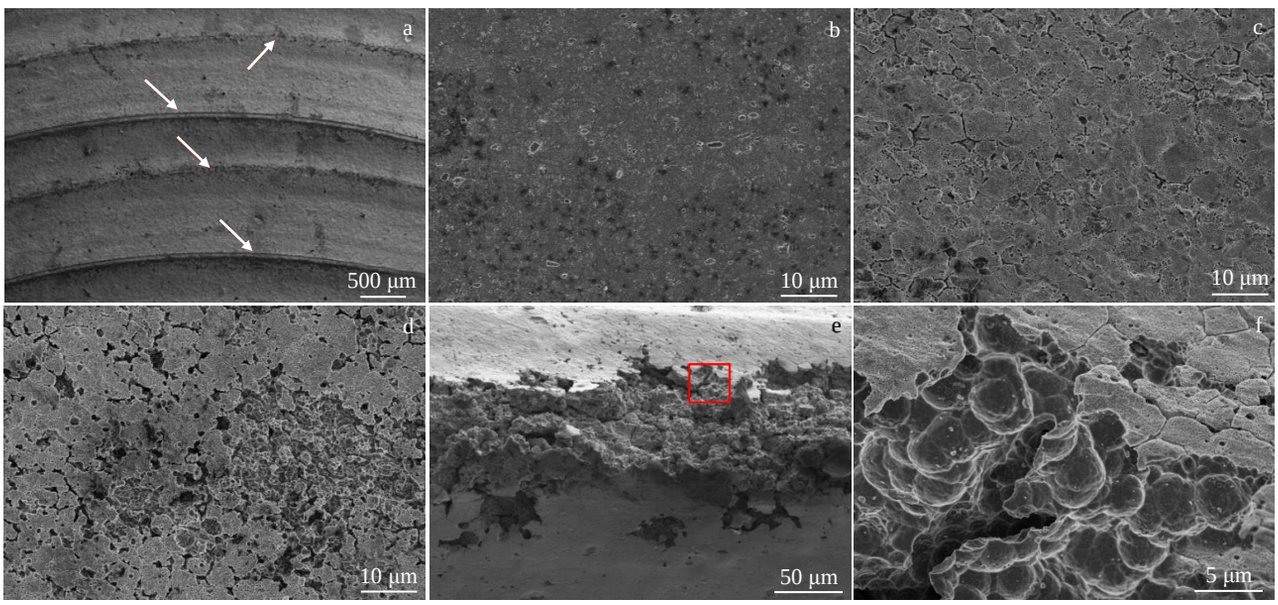

Fig.10 Corrosion morphologies of welded surface before (a) and after immersion corrosion for 2 months (b), 4 months (c), and 6 months (d); microstructure of arc top (e); magnified image of rectangular area in Fig.10e (f)

behavior than other areas do. It can also be found that in the shoulder edge region, the top of the cracked arc undergoes severe corrosion, and the microstructure changes to spherical shape, as shown in Fig.10f.

3 Discussion

The AA2219-T87 aluminum alloys have a high proportion of Cu elements, and the main precipitated phases are the steady-state θ (Al_2Cu) phase and the sub-stable transition θ'' and θ' phases. The interfaces of the sub-stable θ'' and θ' phases have the co-grid or semi-co-grid relationship with the matrix α, while the steady-state θ phase has the completely non-co-grid relationship with the matrix[21,22]. Fig. 11 shows TEM images of different welded regions. It can be seen that the coherent θ'' phase is the dominant phase of BM, and there is a small amount of θ' phase. Fig.11b reveals that there is only θ phase in WNZ, which is affected by heating and mechanical stress. Fig.11c and 11d show the coarse θ' phase in both HAZ-AS and HAZ-RS regions, which are converted from θ'' phase due to the high temperature during the welding process. These results are in agreement with Ref. [23]. The grain boundaries can lead to uneven material properties, and the continuous precipitation of the secondary phase particles along the grain boundaries can further increase the corrosion resistance of materials.

The microhardness at different depths of welded specimen is well related to the microstructure and especially the distribution of the secondary phase particles of specimens. Because of the distribution of dense θ'' and sparse θ' phases, the microhardness of BM is the largest. William et al[24] explained that the formation of θ'' phase significantly improves the strength and hardness of aluminum alloys, followed by the formation of θ' and θ phases. In addition, the welded joints are affected by the thermal cycling, and the transformation from θ'' phase to θ' phase shows coarsening and softening effects in HAZ. The microhardness is decreased from BM to HAZ, while that of WNZ is increased due to the significant grain refinement. Therefore, the microhardness of HAZ is the lowest.

There are dispersed secondary phase particles in Al alloys, which have great effect on the localized corrosion behavior of

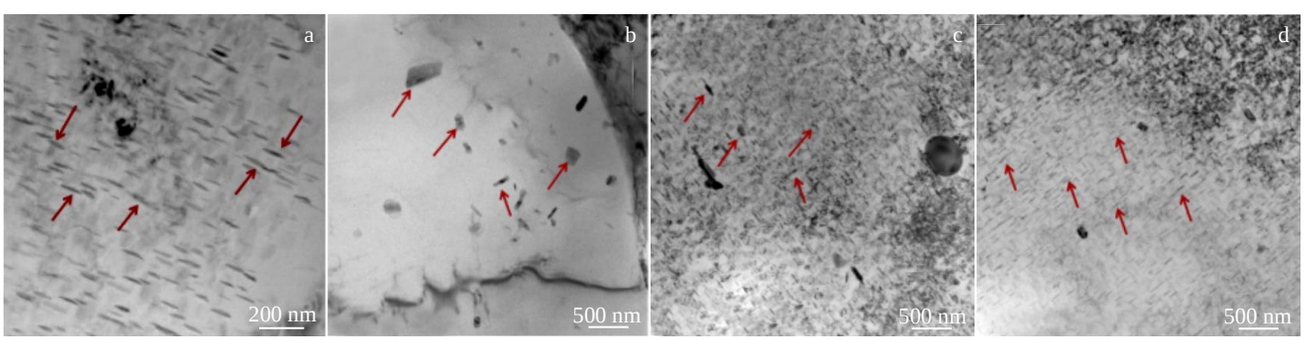

Fig.11 TEM images of BM (a), WNZ (b), HAZ-AS (c), and HAZ-RS (d) regions of welded joints

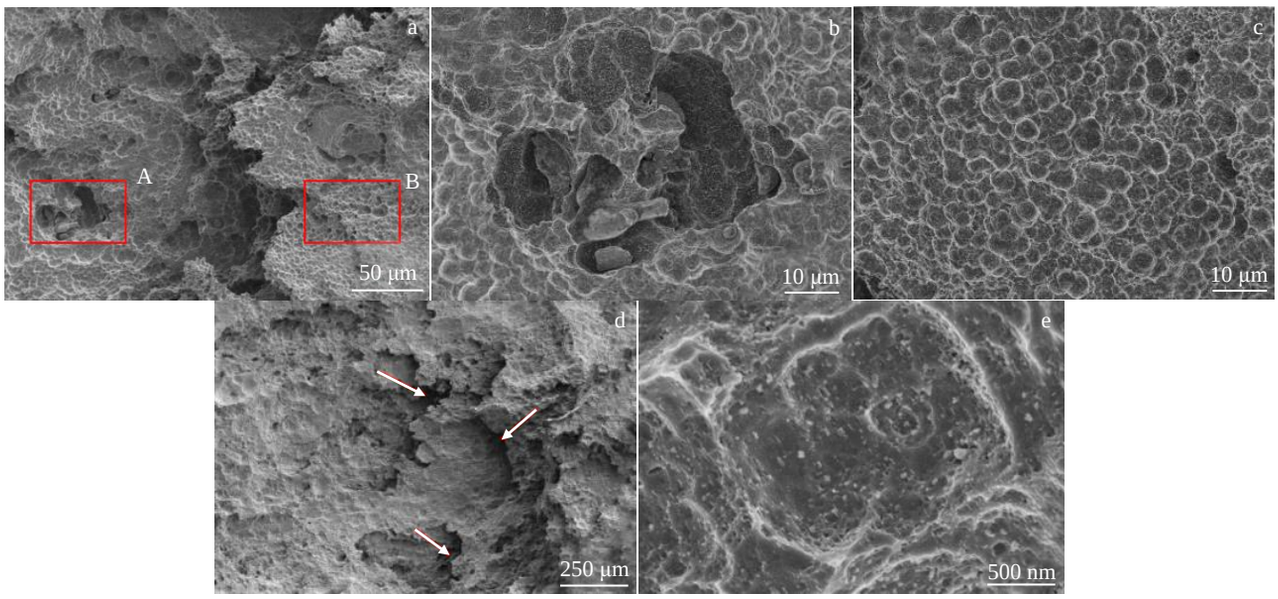

Fig.12 Morphology of etch pits (a) and magnified morphologies of area A (b) and area B (c) in Fig.12a of BM; morphologies of etch pits of BM at low (d) and high (e) magnification

Al alloys[23,25]. The large round black spots in Fig. 11 suggest that the pits may be associated with the secondary phase particles, resulting in the aggregation of the secondary phase particles. Fig. 12a shows the morphology of etch pits after corrosion occurs around the secondary phase particles. Fig. 12b indicates that the etch pits are irregularly shaped, and Fig. 12c indicates that the material of the etch pits has nearly spherical shape after corrosion shedding. Fig. 12d shows that there are deeper pits in the corrosion ditch, resulting in the existence of corrosion fluid and thereby leading to further corrosion along the depth direction. Because the pitting degree along the depth direction is greater than the that along the transverse direction, there are many rod-like or nearly-spherical white particles adhering to the surface of etch pits, as shown in Fig.12e.

Because the corrosion of BM is serious, the corrosion mechanism of BM is analyzed. Many small and shallow etch pits can be found on BM surface after corrosion for 3 weeks, and they expand in both depth and transverse directions with the corrosion proceeding. After 6 months, BM surface is covered with continuous large deep etch pits. Fig. 13 shows the schematic diagrams of corrosion evolution. At the beginning, the surface is immersed in the corrosive liquid, the passivation layer is damaged, and the internal structure is exposed. The potential of the secondary phase particles is higher than that of the peripheral particles, because the secondary phase particles contain copper with high potential. Thus, the exposed surface forms a primary cell due to the potential difference, and the presence of Cl^- accelerates the reaction, leading to higher longitudinal corrosion rate V_{deep} than the transverse corrosion rate V_{width}. The surface pits become bigger and deeper until they are connected to each other, thereby forming large pieces of metal fracture, i.e., the corrosion is developed from pitting to spalling. Therefore, severe corrosion occurs on the surface.

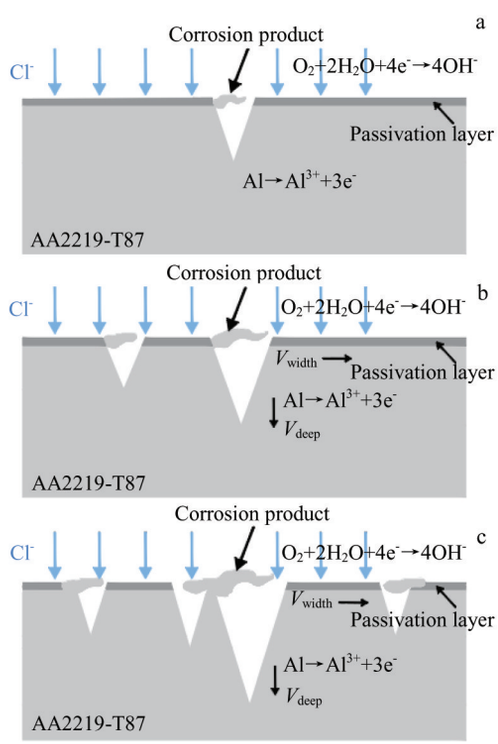

Fig.13 Schematic diagrams of the beginning (a), middle (b), and final (c) stages in corrosion evolution

4 Conclusions

1) The microhardness of AA2219-T87 aluminum alloys is related to the distribution and transformation of strengthening phases. The θ'' phase has the most positive influence on the microhardness, followed by θ' and θ phases. Meanwhile, the

grain refinement also plays an important role in hardness improvement.

2) The potential difference of the base material (BM), heat-affected zone (HAZ)/thermal-mechanically affected zone (TMAZ), and welding nugget zone (WNZ) is −0.71, −0.68, and −0.62 V, respectively. The corrosion potential of BM, HAZ/TMAZ, and WNZ is −0.719, −0.682, and −0.622 V, respectively. The order of corrosion susceptibility is BM> HAZ/TMAZ>WNZ.

3) The severe corrosion occurs on BM surface, and the pits account for 95.17% of the surface area after corrosion for 6 months. The pits become connected to each other. Several obvious etch pits appear on HAZ-advancing side (AS) and HAZ-retreating side (RS) after corrosion for 6 months. WNZ and both sides of the shoulder edge have good corrosion resistance. In the shoulder edge region, the top of the cracked arc undergoes severe corrosion.

4) The potential difference and Cl^- ions are the main reasons for corrosion development of the welded joints. The morphology and distribution of the secondary phase particles can also cause more severe corrosion of BM than that of other areas.

References

1 Mendez P F, Eagar T W. *Advanced Materials & Processes*[J], 2001, 159(5): 39

2 Huang C, Kou S. *Welding Journal*[J], 2000, 79(5): 113

3 Malarvizhi S, Balasubramanian V. *Transactions of Nonferrous Metals Society of China*[J], 2011, 21(5): 962

4 Liu J X, Shen J, Li X W *et al*. *Rare Metal Materials and Engineering*[J], 2019, 48(12): 3797

5 Trueba J L, Torres M A, Johannes L B. *International Journal of Material Forming*[J], 2018, 11(4): 559

6 Hilgert J, Santos J F, Huber N. *Science and Technology of Welding and Joining*[J], 2012, 17(6): 454

7 Dalder E C, Pastrnak J W, Engel J *et al*. *Welding Journal*[J], 2008, 87(4): 40

8 Elanchezhian C, Ramnath B V, Venkatesan P. *Procedia Engineering*[J], 2014, 97: 775

9 Hou J C, Liu H J, Zhao Y Q. *The International Journal of Advanced Manufacturing Technology*[J], 2014, 73(5): 1073

10 Chen Y C, Nakata K. *Materials & Design*[J], 2009, 30(3): 469

11 Kumbhar N T, Sahoo S K, Samaidar I. *Materials & Design*[J], 2011, 32(3): 1657

12 Fuse K, Badheka V. *Science and Technology of Welding and Joining*[J], 2019, 24(4): 277

13 Paglia C S, Buchheit R G. *Scripta Materialia*[J], 2018, 58(5): 383

14 Zhao C Y, Zhang H, Shao T G *et al*. *Corrosion Engineering, Science and Technology*[J], 2019, 54(1): 86

15 Zhang H, Zhao C Y, Cui B *et al*. *Journal of Physics: Conference Series*[J], 2018, 1063: 12 070

16 Zhang Hua, Cui Bing, Lin Sanbao *et al*. *Transactions of the China Welding Institution*[J], 2018, 39(7): 71 (in Chinese)

17 Fonda R W, Bingert J F. *Metallurgical and Materials Transactions A*[J], 2004, 35(5): 1487

18 Chen Y C, Feng J C, Liu H J. *Materials Characterization*[J], 2009, 60(6): 476

19 Yin Z, Chen Y, Yan H *et al*. *Journal of Alloys and Compounds* [J], 2019, 783: 877

20 Fang Zhan, Wang Fan, Yin Yuhuan *et al*. *Rare Metal Materials and Engineering*[J], 2017, 46(7): 2017 (in Chinese)

21 Mondolfo L F. *Structure and Properties of Aluminum Alloys*[M]. London: Butterworths Press, 1976: 200

22 Haasen P. *Physical Metallurgy*[M]. Cambridge: Cambridge University Press, 1978: 183

23 Uyime D, De Viveiros B V G, De Alencar M C *et al*. *Materials Characterization*[J], 2018, 144: 99

24 William J D C. *Fundamentals of Materials Science and Engineering*[M]. Beijing: Chemical Industry Press, 2011

25 Zhang Hua, Sun Datong, Zhang He *et al*. *Rare Metal Materials and Engineering*[J], 2015, 44(1): 103 (in Chinese)

AA2219-T87铝合金双轴肩搅拌摩擦焊的腐蚀行为

邵明皓[1]，张　健[2]，王渭平[3]，刘德博[2]，郭启龙[1]，张　华[1]

(1. 北京石油化工学院 机械工程学院，北京 102617)

(2. 北京宇航系统工程研究所，北京 100076)

(3. 驻成都地区代表室，四川 成都 610100)

摘　要：采用电化学腐蚀和浸泡腐蚀试验对双轴肩搅拌摩擦焊AA2219-T87型铝合金的不同区域进行了腐蚀研究。结果表明，焊缝区具有最高的耐腐蚀性，母材的耐腐蚀性最差。母材中析出相的体积分数最高，越靠近焊核，析出相回溶数量越多。焊核区由细小的等轴晶组成，只存在少量θ相。

关键词：双轴肩搅拌摩擦焊；铝合金；腐蚀行为；耐腐蚀性

作者简介：邵明皓，男，1998年生，硕士生，北京石油化工学院机械工程学院，北京 102617，E-mail：shaominghao123@foxmail.com